



Mimicking multiple stellar populations

G. Nikolov

Institute of Astronomy and National Astronomical Observatory, Bulgarian Academy of Sciences, Tsarigradsko Shose 72, BG-1784, Sofia, Bulgaria
e-mail: gnikolov@astro.bas.bg

Abstract. In recent years there have been observational confirmations of Multiple Stellar Populations in star clusters, interpreted as result of several subsequent bursts of star formation. In this research we show an example of how the observation with multi-chip camera (such as WFPC2 onboard Hubble Space Telescope) and the variations in the data reduction process can result in a broadening of a cluster's Main Sequence by up to 0.25 magnitude. As a testbed we use the LMC star cluster NGC 2031. Since many of the Multiple Stellar Populations are observed in the Magellanic Clouds clusters with multi-chip cameras, the implications of this case on the interpretation of a Main Sequence broadening as multiple episodes of star formation might be quite substantial.

Key words. Star clusters: individual: NGC 2031

1. Introduction

Some of the most impressive objects in the night sky are the dense, glamorous balls of stars known as star clusters. For decades, astronomers have known that stars in star clusters are formed in one episode of star formation so that the stars in a cluster are coeval. However, recent discoveries of young stars in old clusters have changed these concepts (Gratton et al. 2012; Girardi et al. 2009). Extended main sequences and multiple stellar populations have been identified in many intermediate-age star clusters in the neighbouring Magellanic Clouds galaxies, but the interpretation is still unclear (Niederhofer et al. 2015; Cabrera-Ziri et al. 2015; Bastian et al. 2016).

In this paper we use WFPC2 images to show an example when observing with multi-

CCD camera can mimic a split in a cluster's main-sequence.

2. Observations

In this work we use archival observations of the cluster NGC 2031 from the Hubble Space Telescope WFPC2 camera, obtained from the STScI¹ archive. We use observations in two HST filters, namely F555W and F814W, which correspond to Johnson's V and I. The different exposure times ensure that both bright and faint stars are well exposed and not saturated. Only the best-quality images were used from proposal ID 5904 (PI: Fischer). Details on the particular datasets used are described in Table 1.

¹ <http://archive.stsci.edu>

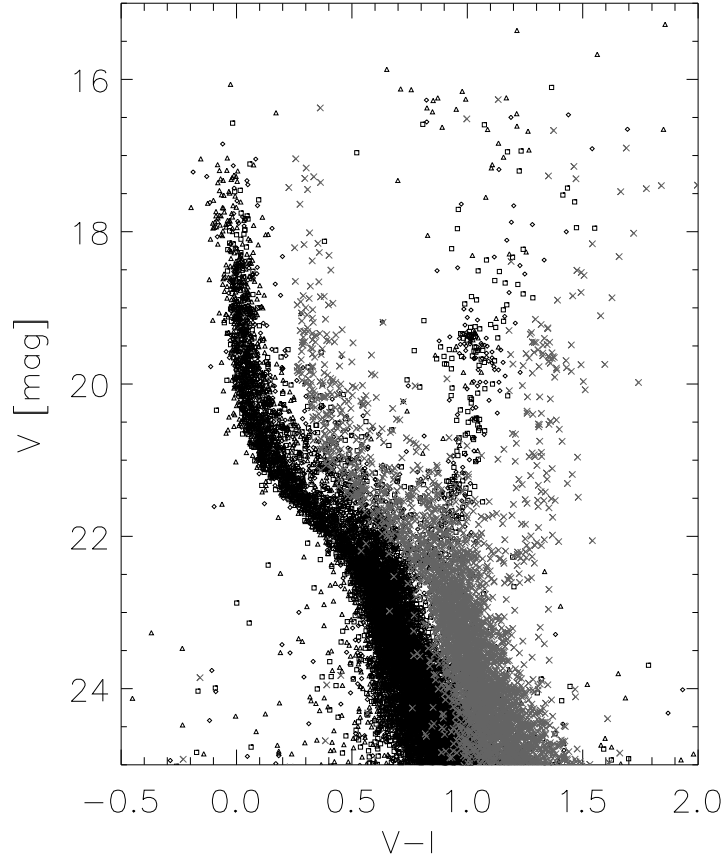


Fig. 1. CMD of the cluster NGC 2031 in standard filters V and I with stars from different WFPC2 CCDs denoted: PC as triangle, WF2 as diamond, WF4 as square, and WF3 as x and grey in colour.

3. Photometry

The photometry was done using *HSTphot*² (Dolphin 2000) - a package designed especially for simultaneous PSF photometry of multiple WFPC2 images. The calibrated images were first masked by data-quality mask to reject bad pixels with already known defects, such as permanent camera defects, bad pixels, unrepaired warm pixels, etc.

Then the image sky level is determined using the routine *getsky* - for each pixel the mean of its neighbouring pixels in an annulus around

² <http://americano.dolphinim.com/hstphot/>

it. The sky level is recomputed also during the photometry to ensure better estimation.

The cosmic rays are removed from the images with the same positioning and filter by the routine *crmask*, which then are combined to produce a single clean image to be used for the photometry. The individual images were separated in groups by filter, exposure time and positioning. All those were then run through the *HSTphot* cosmic-ray rejection routine, *crmask*, which identifies cosmic rays on a pixel-by-pixel basis and flags cosmic rays by looking for pixels whose values significantly exceed those in other observations in the set.

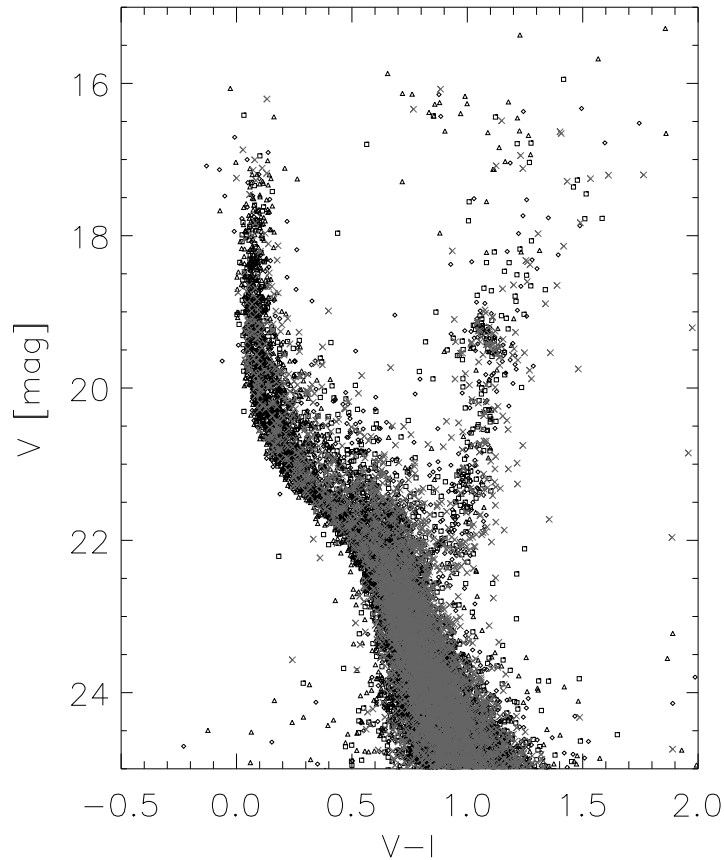


Fig. 2. Same as Figure 1, no local sky determination.

The photometric solutions were done by the routine *hstphot* with detection threshold of 5σ . During the photometry two options have been used. The first does artificial star tests and we added more than half a million artificial stars to estimate the completeness of the photometric data. The second re-fits the sky during the photometry, which is recommended for general use in the HSTphot manual.

3.1. Sky level determination

In fields with rapidly-varying background or crowded regions it is recommended to estimate a local sky for each individual star just outside the photometry aperture. A drawback

of this method is that it overestimates the sky background near brightest stars. Our experimenting showed that the background in the images used is not rapidly-varying on small scales of arcsec to demand a local sky determination. Alternatively we can measure the global sky background for the whole CCD, a varying mean for each pixel, and produce a global sky level map for the camera.

In this study we did two runs of the photometric measurements - one with local and other with global sky level determination. The resulting photometry lists are compared below.

After the photometric measurements the positions of the objects were corrected for the geometric distortions of the camera using

Table 1. List of observations used.

dataset name	exptime sec	filter name
u2y80301t	F555W	300
u2y80302t	F555W	300
u2y80303t	F555W	300
u2y80304p	F814W	300
u2y80305p	F814W	300
u2y80306p	F814W	300
u2y80307p	F814W	300
u2y80308p	F814W	300
u2y80309p	F555W	300
u2y8030ap	F555W	300
u2y8030bp	F555W	10
u2y8030cp	F555W	10
u2y8030dp	F814W	10

Holtzman et al. (1995) corrections by the routine *distort*.

3.2. Data quality

For each photometered object HSTphot provides position, χ of the fit, signal-to-noise, sharpness, roundness, major axis, crowding and object type, which are useful for distinguishing between stars and other objects. On the output photometry list we apply a data quality selection. We keep only stellar objects with good photometry and reject objects which do not cover the quality criteria, namely: to have acceptable signal-to-noise ratio (i.e. non-zero), to be classified as a type star with sharpness between -0.3 and 0.3 . The simulated artificial stars are run through the same data quality as the real stars.

4. Discussion

The constructed CMD is presented in Figure 1 for photometry with local sky determinations. The four WFPC2 CCDs are illustrated with different symbols for visibility, and stars lying on the WF3 CCD only are coloured in grey. In this case the WF3 stars are shifted with respect to the other three CCDs stars, broadening the main-sequence and mimicking an older

Table 2. Aperture corrections mean determined for the four CCDs of WFPC2 in magnitudes.

WFPC2 CCD	local sky	global sky
PC	0.377	0.102
WF2	0.134	0.046
WF3	0.343	0.047
WF4	0.167	0.048

population in the cluster, or extended main-sequence turn-off. We use images of different exposure times, so the shift is well visible in both bright and faint stars.

For comparison, the CMD of the cluster when estimating the sky level globally during photometry is presented in Figure 2. In this case the stars from all CCDs of the camera are distributed in the same areas of the CMD, with no apparent shifts.

The root of this discrepancy is in the aperture corrections erroneously determined when local sky for the stars is computed. In Table 2 are listed the aperture corrections applied to the photometry in cases of local and global sky determined. When the sky is considered locally then the aperture corrections are overestimated by the order of $0.20 - 0.25$ magnitudes, reaching 0.30 in WF3. This results in shift on the CMD, as seen in Figure 1. The spread in colour of the main sequence in Figure 2 is much smaller, making the features on the CMD much prominent.

5. Conclusions

Many of the cameras nowadays used with the modern telescopes are a mosaic of several CCD sensors, e.g. WFC3 (Dressel, L., 2017), SDSS (Gunn et al. 1998), Gaia (de Bruijne et al. 2010), and other. In this contribution we show how important it is to consider the whole camera as one, though dealing with individual CCD sensors. The results on objects on the sky should be independent of the imaging equipment.

Acknowledgements. GN would like to express the deepest gratitude to Prof. M. Kontizas and E. Kontizas for the guidance and mentoring. This work is financially supported by the Program for career development of young scientists of Bulgarian Academy of Sciences under contract DFPN-107 and partially supported by the Bulgarian National Science Fund of the Ministry of Education and Science, DN 08-1/2016. Some/all of the data presented in this paper were obtained from the Mikulski Archive for Space Telescopes (MAST). STScI is operated by the Association of Universities for Research in Astronomy, Inc., under NASA contract NAS5-26555.

References

- Bastian, N., Niederhofer, F., Kozhurina-Platais, V., et al. 2016, *MNRAS*, 460, L20
- Cabrera-Ziri, I., Bastian, N., Longmore, S. N., et al. 2015, *MNRAS*, 448, 2224
- de Bruijne, J., Kohley, R., & Prusti, T. 2010, *Proc. SPIE*, 7731, 77311C
- Dolphin, A. E. 2000, *PASP*, 112, 1383
- Dressel, L. 2017, *Wide Field Camera 3 Instrument Handbook, Version 9.0 (STScI, Baltimore)*
- Girardi, L., Rubele, S., & Kerber, L. 2009, *MNRAS*, 394, L74
- Gratton, R. G., Carretta, E., & Bragaglia, A. 2012, *A&A Rev.*, 20, 50
- Gunn, J. E., Carr, M., Rockosi, C., et al. 1998, *AJ*, 116, 3040
- Holtzman, J. A., Burrows, C. J., Casertano, S., et al. 1995, *PASP*, 107, 1065
- Niederhofer, F., et al. 2015, *A&A*, 575, A62